Analysis of BPLC behavior under adverse conditions: A Pathway towards cable health monitoring

Amirali Mahjoob*, Sebastian Tan*, Philipp Lutat*, Andreas Ulbig*†
*IAEW, RWTH Aachen University, Aachen, Germany
{a.mahjoob, p.lutat, a.ulbig}@iaew.rwth-aachen.de; sebastian.tan@rwth-aachen.de
†Fraunhofer FIT, Aachen, Germany

***Abstract*—Broadband Power Line Communication (BPLC) is a promising solution for data exchange and condition monitoring in low-voltage (LV) distribution networks. However, variations in cable properties under thermal or mechanical stress can degrade signal quality and reliability. This work experimentally investigates the behavior of LV power cables under adverse conditions—elevated temperature, mechanical pressure, and electrical faults—to evaluate their impact on BPLC signal propagation. Laboratory measurements were conducted using a modified 2-port Vector Network Analyzer (VNA) setup with controlled heating. The derived line parameters (R', L', G', C', and ε_r) were modeled as functions of frequency and temperature using multivariate regression and neural networks. Results show an exponential increase in R', G', and ε_r with rising temperature, indicating up to 40% higher dielectric losses between $20^\circ\mathrm{C}$ and $80^\circ\mathrm{C}$, while mechanical stress had negligible impact. A frequency-domain impedance method successfully locates short-circuit faults with less than 5% error. These findings support the use of BPLC signals as a low-cost diagnostic and condition-monitoring tool in smart grids.**

***Index Terms*—Broadband Power Line Communication, Smart Grids, Cable Condition Monitoring, Temperature Effects, Fault Localization**

I. Introduction

The growing penetration of distributed energy resources and digital loads are increasing the stress on low-voltage (LV) distribution networks, raising the need for continuous monitoring and reliable communication infrastructures [1]. Broadband Power Line Communication (BPLC) has emerged as an attractive option for data exchange and system diagnostics, as it utilizes existing cables for high-speed communication without additional wiring [2]. However, the transmission characteristics of power lines are highly sensitive to variations in cable parameters, which can be affected by temperature, mechanical stress, and electrical faults [3]–[5]. These variations can distort signal propagation, degrade communication reliability, and complicate network operation.

To ensure robust BPLC performance and enable condition monitoring, a detailed understanding of the frequency- and temperature-dependent behavior of LV cable parameters is required [6]. This paper experimentally investigates these effects under controlled laboratory conditions and evaluates their implications for broadband PLC-based diagnostics in smart grids.

Several studies [7]–[11] have demonstrated the potential of BPLC for autonomous cable health monitoring and degradation detection. Machine learning approaches, including Support Vector Machines and Neural Networks, have also been explored for fault classification and intrusion detection at the physical layer [12]–[14]. In parallel, research initiatives such as the "Fühler im Netz 2.0" project [15] highlight the integration of smart sensors, real-time analytics, and predictive maintenance within distribution networks.

While these efforts demonstrate the diagnostic potential of BPLC systems, the majority of existing work focuses on signal-level analysis or data-driven algorithms rather than on the underlying high-frequency behavior of power cables. In particular, the influence of adverse conditions—such as temperature variations, mechanical stress, and electrical faults—on frequency-dependent cable parameters remains insufficiently understood. Furthermore, field data rarely allow controlled isolation of such effects, making it difficult to systematically evaluate their impact on PLC signal propagation and grid diagnostics.

This work addresses these gaps by developing a physically grounded model of low-voltage power cables based on measured high-frequency S-parameters. The extracted line parameters provide deeper insight into the conductive and dielectric behavior of the cables, enabling improved understanding of signal attenuation mechanisms relevant for BPLC transmission quality. In addition, a series of controlled laboratory test cases is conducted to investigate how elevated temperature, mechanical loading, and short-circuit faults alter the cable parameters. These experiments allow systematic observation of degradation phenomena that are difficult to isolate in field conditions and demonstrate the potential of PLC-based measurements for temperature monitoring, fault detection, and predictive maintenance in smart grids [16].

The remainder of this paper is organized as follows. Section II outlines the theoretical background and the high-frequency techniques applied. Section III describes the measurement setup, experimental procedures, and test cases. Section IV presents and discusses the key results, including parameter modeling and fault localization. Finally, Section V

This work was supported by the German Federal Ministry of Education and Research (BMBF) under project agreement No. 100623731 (PICNIC).

979-8-3315-8138-1

summarizes the main findings and provides an outlook on future research directions.

II. Theoretical Basics

In this section, fundamentals of high-frequency techniques are introduced. This includes the high-frequency line parameters, S-parameters and electro-physical quantities related to this work. The behavior of electrical currents in conductors differs significantly at high frequencies compared to low frequencies or under DC conditions. Two key phenomena in high-frequency conduction, namely the skin effect and proximity effect, play a significant role and need to be considered thoroughly in broadband PLC systems, where the signals are transmitted over a wide frequency range [17].

A. High-Frequency Techniques

This subsection introduces the fundamental concepts and theoretical background relevant to the high-frequency measurement techniques employed in this paper.

1) S-Parameters: Scattering parameters (S-Parameters) are used to characterize and obtain information about the behavior of a two-port system [18].

2) Reflection Coefficient: When an electromagnetic wave passes through two different media, only part of it is transmitted, while the remainder is reflected back to the source. The proportions of the reflection and transmission depend on the respective impedances and can be expressed as:

$$\Gamma = \frac{Z_2 - Z_1}{Z_2 + Z_1}. \tag{1}$$

The transmission factor follows as

$$T = 1 + \Gamma. \tag{2}$$

Three special cases arise from (1) [19]: short-circuit ($Z_2 = 0 \Rightarrow \Gamma = -1$), open-circuit ($Z_2 = \infty \Rightarrow \Gamma = 1$), and perfect matching ($Z_2 = Z_1 \Rightarrow \Gamma = 0$).

3) Input Impedance: The input impedance Z_{in} of a transmission line is the equivalent impedance seen at the line terminals. For a lossy line, one obtains:

$$Z_{in} = Z_w \frac{Z_L + Z_w \tanh(\gamma l)}{Z_w + Z_L \tanh(\gamma l)}, \tag{3}$$

where Z_w is the characteristic impedance, Z_L is the load impedance, and γ is the propagation constant.

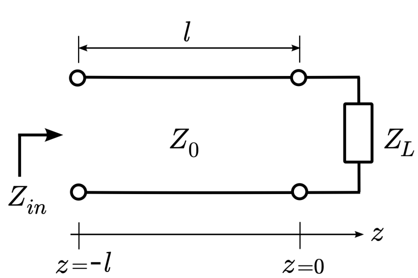

Fig. 1: A transmission line driven by a source on the left and terminated by a load impedance Z_L on the right [19].

4) High-Frequency Line Parameters: In high-frequency technology, the dimensions of a transmission line are small relative to the wavelength ($\lambda \gg l$) [19], [20]. The line is modeled using infinitesimal segments with distributed parameters.

a) Characteristic impedance Z_w: Defined as the ratio of voltage to current of a forward-traveling wave [18]:

$$Z_w = \sqrt{\frac{R' + j\omega L'}{G' + j\omega C'}}. \tag{4}$$

b) Propagation constant γ: A complex, frequency-dependent quantity describing attenuation and phase shift [20]:

$$\gamma = \sqrt{(R' + j\omega L')(G' + j\omega C')} = \alpha + j\beta, \tag{5}$$

where α is the attenuation constant and β the phase constant.

c) Velocity factor: The ratio between propagation speed and the speed of light:

$$v_f = \frac{1}{\sqrt{\varepsilon_r \mu_r}} = \frac{2\pi f}{\beta c_0}. \tag{6}$$

d) Relative permittivity ε_r: For non-magnetic materials ($\mu_r \approx 1$):

$$\varepsilon_r \approx \frac{1}{v_f^2}. \tag{7}$$

e) Primary line parameters: The distributed parameters R', L', G', and C' describe conductor losses, magnetic energy storage, dielectric leakage, and electric field storage, respectively.

B. Parameter Extraction from S-Parameters

The two-port VNA provides the complex scattering parameters S_{11} and S_{21}, from which the propagation constant γ and characteristic impedance Z_c are obtained through a standard transmission-line inversion. A complete derivation is given in our earlier work. The following section describes the laboratory setup and test scenarios used to collect the S-parameter data from which the line parameters are extracted.

III. Methodology

This section describes the laboratory measurement methodology used in this work.

A. Reflection Measurements

Reflection measurements were performed using open-circuit ($\infty\,\Omega$) and short-circuit ($0\,\Omega$) terminations to determine the line parameters under different load conditions.

B. Transmission Measurements and Temperature Variation

The transmission measurements were performed to validate the extracted line parameters. Two conductors were connected to a programmable current source for heating (Fig. 2), while the remaining two formed the VNA measurement path (Fig. 3). Cable temperature was monitored using thermocouples and verified with an infrared camera. The current was adjusted to reach and maintain the target temperature during the short VNA sweep. Four scenarios were tested: (i) room temperature,

979-8-3315-8138-1

(ii) elevated temperature, (iii) mechanical compression, and (iv) short-circuit faults.

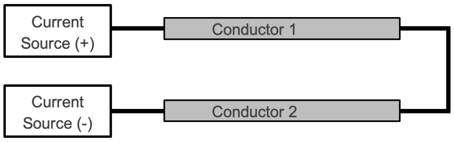

Fig. 2: Schematic of connection between cable and current source.

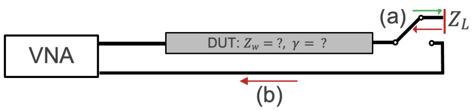

Fig. 3: Test setup for (a) reflection measurements and (b) transmission measurements.

C. Test Cases

The main objective was to investigate how temperature and fault conditions influence the cable parameters. In addition to elevated-temperature tests, two representative real-life fault scenarios were examined.

1) Fault – Mechanical Pressure: Situations may occur where cables are subjected to higher-than-normal mechanical pressure, potentially altering their electrical characteristics.

2) Fault – Short Circuit: During construction work, power cables may be unintentionally damaged by drilling or cutting, resulting in short-circuit faults.

3) Fault – Very High Temperature: Short-circuit or over-current conditions can cause rapid and extreme heating. PVC-insulated cables are typically rated up to 80 °C; above this limit, chemical changes may occur in the insulation layers. While these effects are not easily detectable with low-frequency measurements, the resulting dielectric changes may become observable in the high-frequency domain.

D. Data Analysis

1) Raw Data: To better visualize the parameter dependencies and reduce measurement noise, the raw extracted parameters were processed using interpolation and surface-modeling techniques. Figure 5 compares the raw data with the Neural Network and multivariate regression surfaces.

First, the line parameters are directly extracted from the raw S-parameter data using the relations in Section II-B. The parameters are visualized as 3D surface plots and then interpolated to produce a higher-resolution input for modeling.

2) Surface Modeling: Two modeling methods were implemented to smooth measurement noise and obtain continuous dependencies: a Neural Network and a Multivariate Regression. Three metrics were used to evaluate model accuracy: Mean Squared Error (MSE), Mean Absolute Percentage Error (MAPE), and the Coefficient of Determination (R^2).

a) Neural Network: The neural network consists of multiple interconnected layers that apply weighted transformations and activation functions to identify potential nonlinear patterns in the data.

b) Multivariate Regression: The multivariate regression model estimates parameter dependencies using the function:

$$\text{Parameter}(f, T) = e^{\theta_0+\theta_1 f+\theta_2 T+\theta_3 f^2+\theta_4 fT+\theta_5 T^2}. \quad (8)$$

3) Fault Analysis: In addition to temperature-dependent behavior, the characteristics of faulted cables and the potential for fault-location using frequency-domain measurements were also investigated.

IV. Exemplary Results and Discussion

This section presents the measured high-frequency line parameters under varying temperature and fault conditions.

A. Temperature Dependency of Line Parameters

Fig. 4 shows the 4 main parameters of the cables for different range of frequency and Temperature. The measured data show that the series resistance (R') and shunt conductance (G') increase significantly with temperature. This behavior arises from the rise in conductor resistivity and dielectric losses in the insulation at elevated temperatures. In contrast, the inductance (L') and capacitance (C') exhibit only weak or inconsistent changes, as they primarily depend on cable geometry and material permittivity, which are less sensitive to thermal effects. The small observed deviations for L' and C' are within the expected range of measurement uncertainty and frequency dispersion.

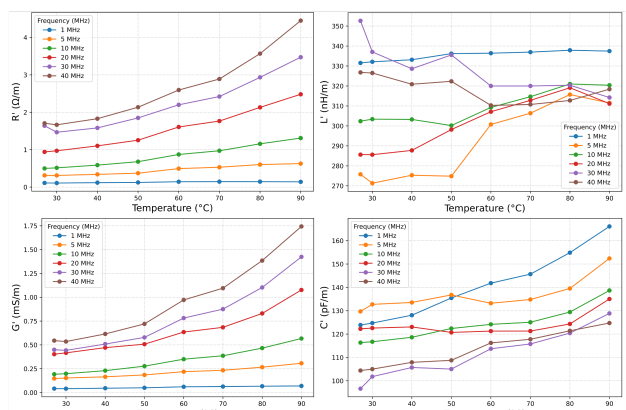

Fig. 4: Raw extracted line parameters: (a) top-left: R' increases with both f and T; (b) top-right: L' remains nearly constant; (c) bottom-left: C' shows slight thermal variation; (d) bottom-right: G' rises with temperature due to dielectric losses.

Figure 4 shows the extracted line parameters over frequency and temperature. The series resistance R' and shunt conductance G' increase clearly with both frequency and temperature due to higher conductor resistivity and rising dielectric losses at elevated temperatures, as well as skin-effect–related current redistribution. In contrast, the inductance L' and capacitance

979-8-3315-8138-1

C' vary only slightly, since they are mainly determined by geometry and dielectric permittivity, which change little with temperature. The small fluctuations in L' and C' are attributed to measurement uncertainty and frequency dispersion.

B. Surface Modeling

As mentioned, Neural Network and Multivariate Regression methods have been used to create surfaces to observe the dependency of parameters to temperature and frequency simultaneously. Fig. 5 compare these two methods. While the Neural Network surface provides more details, it is difficult to use for other purposes due to its complexity. The Multivariate Regression surface shows the increasing nature of R and G with both temperature and frequency.

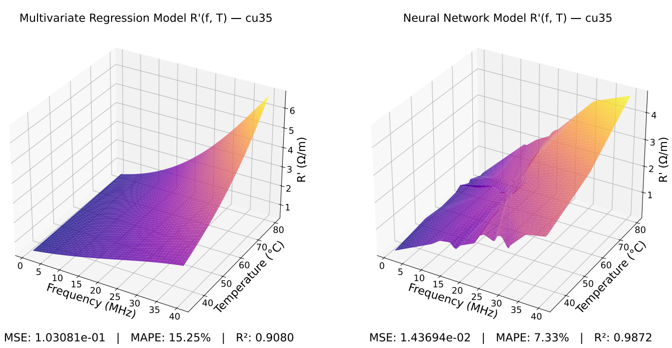

Fig. 5: Comparison of Regression VS. Neural Network surface

The following subsection presents the measured responses under fault conditions and evaluates their diagnostic relevance for PLC-based monitoring.

C. Faults

The following fault tests were performed under laboratory conditions at approximately 30–35 °C.

1) External Pressure: Both mechanical-pressure tests showed no observable changes in the line parameters. This is expected, as the applied pressure mainly affects the outer PVC sheaths, while the core insulation—and thus the electromagnetic field distribution—remains largely unchanged. Higher pressures may lead to measurable effects, particularly because NAYY cables consist of three PVC layers of which only the innermost one significantly influences high-frequency signal transmission [17].

2) Short Circuit: For short-circuit tests, a 32 m Cu4x35 mm^2 cable was used. A screw was driven into the cable at approximately 22 m, directly shorting the two measurement conductors. Consequently, all four measurement configurations (short, open, 50 Ω, gain) collapsed to the short-circuit response, as shown in Fig. 6(a). Although not representative of the cable's true behavior, this condition is suitable for fault-location analysis.

Afterward, the screw was removed, leaving only local sheath damage. The resulting parameters (Fig. 6(b)) show small reductions in R', L', G', and C', while the relative permittivity ε_r remains essentially unchanged. Since ε_r is primarily a material property, this indicates that the core dielectric was not significantly altered.

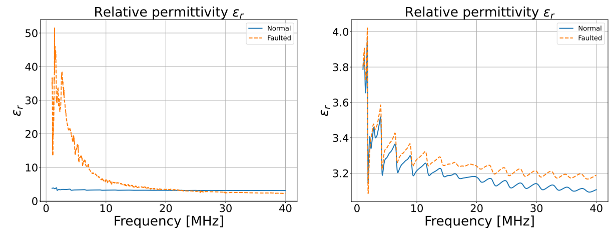

Fig. 6: Relative permittivity for (a) shorted cable and (b) damaged cable.

Overall, mechanical compression has minimal influence on the high-frequency parameters, whereas short-circuit damage produces clear deviations due to local insulation breakdown and conductor contact. These changes are also visible in the input-impedance trace, enabling the fault-location technique described below.

3) Fault Location: With the screw in place, the fault creates a closed short-circuit loop, causing all measurement types to coincide. The resulting input impedance is shown in Fig. 7.

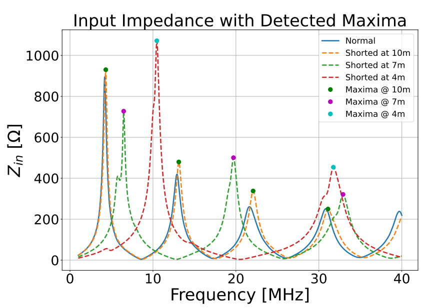

Fig. 7: Measured input impedance of shorted cable.

The fault location is determined by:

1) identifying the maxima in Fig. 7,
2) computing the average spacing Δf,
3) deriving the faulted velocity factor $v_{f,\text{faulted}} = 2l\Delta f/c_0$,
4) estimating the distance $x = (v_{f,\text{faulted}}/v_{f,\text{normal}})\,l$.

The computed faulted velocity factor is shown in Fig. 8; the estimated fault location is 21.06 m, compared with the actual 22 m.

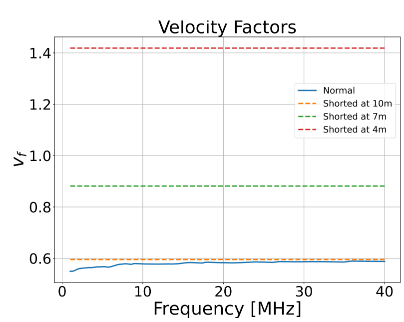

Fig. 8: Normal vs. faulted velocity factor.

To verify the method, a 10 m Cu4x16 mm^2 cable was tested with faults at approximately 10 m, 7 m, and 4 m. The estimated locations and errors are shown in Table I.

Fault location	Calculated location	Error margin
22 m	21.06 m	4.27%
10 m	9.88 m	1.20%
7 m	6.67 m	4.71%
4 m	4.14 m	3.50%

TABLE I: Results and error of fault location

4) Extra High Temperature: High-temperature tests were performed to evaluate extreme thermal degradation. The results in Fig. 9 show that very high temperatures significantly affect the dielectric properties above 30 MHz. Such effects are critical because overheated insulation softens and becomes more susceptible to mechanical damage or subsequent faults. The results show that extreme heating leads to a measurable reduction in dielectric performance at high frequencies.

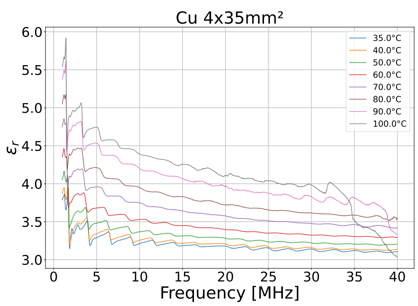

Fig. 9: Relative permittivity at high temperatures.

V. Discussion and Conclusion

The results show a clear temperature- and frequency-dependent increase in the resistive parameters R' and G', caused by higher conductor resistivity and increased dielectric losses. In contrast, L' and C' vary only weakly, as they are mainly governed by geometry and dielectric permittivity; the small fluctuations are attributed to measurement noise, dispersion, and environmental influences.

Unlike previous work that focused on signal-level attenuation, this study extracts the full RLGC parameter set, enabling a more physical interpretation of how adverse conditions affect PLC channels. Regression-based surface modeling further provides smooth temperature–frequency dependencies.

The accuracy of the results is constrained by non-uniform heating, surface temperature sensing, VNA noise, and the simplified regression model. Still, the high-frequency parameters proved diagnostically meaningful: short-circuit faults produced characteristic impedance signatures that enabled fault-location estimates within a few percent, while high-temperature tests revealed dielectric changes above 30 MHz indicative of early insulation degradation.

Overall, combining S-parameter measurements, RLGC extraction, and data-driven modeling provides a low-cost, non-invasive basis for PLC-based cable monitoring. The approach shows potential for thermal estimation and fault detection. Future work should address additional fault types, long-term aging, and improved models to support predictive maintenance in distribution networks.

References

[1] K. P. Guddanti, A. K. Bharati, S. Nekkalapu, J. Mcwherter, and S. Morris, "A comprehensive review: impacts of extreme temperatures due to climate change on power grid infrastructure and operation," *IEEE Access*, 2025.

[2] K. Sharma and L. M. Saini, "Power-line communications for smart grid: Progress, challenges, opportunities and status," *Renew. Sustain. Energy Rev.*, vol. 67, pp. 704–751, 2017.

[3] A. Bosisio *et al.*, "Extreme weather conditions effects on underground cable joints failures: Strategies for reliability and resilience improvement," in *Proc. CIRED 2021 – 26th Int. Conf. Exhib. Electricity Distribution*, 2021, pp. 91–94.

[4] P. Lutat, M. Kurth, and A. Ulbig, "Temperature and frequency behavior of low voltage cables for broadband powerline applications," in *Proc. IEEE Int. Symp. Power Line Commun. Appl. (ISPLC)*, 2023, pp. 13–18.

[5] F. Gruber, "Degradation detection on power lines using power line communication devices," Ph.D. dissertation, Dissertation, Erlangen, Friedrich-Alexander-Universität Erlangen-Nürnberg ..., 2019.

[6] P. Lutat, J. Girbig, S. Bouchkati, and A. Ulbig, "Modelling latencies of broadband powerline communication networks for smart grids," in *2024 IEEE PES Innovative Smart Grid Technologies Europe (ISGT EUROPE)*. IEEE, 2024, pp. 1–6.

[7] L. Förstel and L. Lampe, "Grid diagnostics: Monitoring cable aging using power line transmission," in *Proc. IEEE Int. Symp. Power Line Commun. Appl. (ISPLC)*, 2017, pp. 1–6.

[8] Y. Huo, G. Prasad, L. Atanackovic, L. Lampe, and V. C. M. Leung, "Grid surveillance and diagnostics using power line communications," in *Proc. IEEE Int. Symp. Power Line Commun. Appl. (ISPLC)*, 2018, pp. 1–6.

[9] ——, "Cable diagnostics with power line modems for smart grid monitoring," *IEEE Access*, vol. 7, pp. 60 206–60 220, 2019.

[10] L. Benesl, P. Mlynek, M. Ptacek, V. Vycital, J. Misurec, J. Slacik, M. Rusz, and P. Musil, "Cable monitoring using broadband power line communication," *Sensors*, vol. 22, no. 8, 2022.

[11] Y. Huo, "Cable health monitoring using power line communications signal and machine learning technique," Ph.D. dissertation, University of British Columbia, 2023.

[12] G. Prasad, Y. Huo, L. Lampe, and V. C. M. Leung, "Machine learning based physical-layer intrusion detection and location for the smart grid," in *Proc. IEEE Int. Conf. Commun., Control, Comput. Technol. Smart Grids (SmartGridComm)*, 2019, pp. 1–6.

[13] Y. Huo, G. Prasad, L. Lampe, and V. C. M. Leung, "Advanced smart grid monitoring: Intelligent cable diagnostics using neural networks," in *Proc. IEEE Int. Symp. Power Line Commun. Appl. (ISPLC)*, 2020, pp. 1–6.

[14] Y. Huo, G. Prasad, L. Lampe, V. C. M. Leung, R. Vijay, and T. V. Prabhakar, "Measurement-aided training of machine learning techniques for fault detection using plc signals," in *Proc. IEEE Int. Symp. Power Line Commun. Appl. (ISPLC)*, 2021, pp. 78–83.

[15] C. Balada, S. Ahmed, A. Dengel, M. Bondorf, N. Hopfer, and M. Zdrallek, "Fühler-im-netz: A smart grid and power line communication data set," *IET Smart Grid*, 2022.

[16] T. K. Queder, J. Hampel, and A. Mahjoob, "Development of a monitoring system for assessing the condition of low-voltage cables based on broadband powerline communication," in *ETG Kongress 2025; Voller Energie–heute und morgen*. VDE, 2025, pp. 485–491.

[17] A. Mahjoob, Y. Liu, S. Bouchkati, and A. Ulbig, "Investigation of characteristics of cables in high frequency for power line communication using finite element analysis," in *2024 IEEE PES Innovative Smart Grid Technologies Europe (ISGT EUROPE)*. IEEE, 2024, pp. 1–5.

[18] R. B. Keller, *Design for Electromagnetic Compatibility—In a Nutshell: Theory and Practice*. Cham, Switzerland: Springer International Publishing AG, 2023.

[19] S. W. Ellingson, *Electromagnetics, Vol. 1*. Blacksburg, VA: VT Publishing, 2018. [Online]. Available: https://doi.org/10.21061/electromagnetics-vol-1

[20] H. Johnson and M. Graham, *High-Speed Signal Propagation: Advanced Black Magic*. NJ, USA: Prentice Hall Press, 2003.

979-8-3315-8138-1